Increasing Trend on Storm Wave Intensity in the Western Mediterranean

Khalid Amarouche [ID] **and Adem Akpınar *** [ID]

Department of Civil Engineering, Bursa Uludağ University, Gorukle Campus, 16059 Bursa, Turkey;
khalidamarouche@uludag.edu.tr
* Correspondence: ademakpinar@uludag.edu.tr; Tel.: +90-532-486-95-71

Abstract: Annual trends in storm wave intensity over the past 41 years were evaluated during the present study. Storm wave intensity is evaluated in terms of total storm wave energy (TSWE) and storm power index (SPI) of Dolan and Davis (1992). Using an accurate long-term wave hindcast developed using a calibrated SWAN model, all storm wave events occurring over the past 41 years were characterized in terms of significant wave height (H_s) and total storm duration. Thus, both SPI and TSWE was computed for each storm wave event. The Theil–Sen slope estimator was used to estimate the annual slopes of the SPI and TSWE and the Mann–Kendall test was used to test the trend significance with different confidence levels. The present study is spatially performed for the western Mediterranean Sea basin considering 2308 grid points in a regular grid of 0.198° resolution in both directions. Results allow as to define five hotspots covering a large area, experienced a significant increasing slope in both SPI and TSWE (annual maxima and average). The confidence level in this area exceed 95%, with a steep slope between 100 kWh·m^{-1}·year^{-1} and 240 kWh·m^{-1}·year^{-1} for annual max TSWE and between 28 m^2·h·year^{-1} and 49 m^2·h·year^{-1} for annual max SPI. Consideration of the present findings is strongly recommended for risk assessment and for sustainable development in coastal and offshore area and to identify areas sensitive to global climate change in the western Mediterranean Sea.

Keywords: wave modeling; storm wave intensity; total storm wave energy; storm power index; trend; Western Mediterranean Sea

1. Introduction

Marine storms are one of the major preoccupations of sea users and marine security services. They are often responsible for significant damage and loss in several sectors of marine activity such as aquaculture [1] and navigation [2,3]; additionally, these storms are responsible for several changes in the coastlines [4,5] and cause damage to coastal and port infrastructure [6–8]. The extent of this damage can have a considerable impact on the economies of countries. Currently, several researchers are interested in assessing the impact of storms on coastal areas in the Mediterranean [9–15]. These contributions have been motivated by the alarming climate changes observed over the last decades [5,16–18], considering the increasing trend in significant wave heights (H_s) reported in several studies [19–24], as well as the increase in Hs during tropical cyclones [25,26], and also the variation in storm wave intensity [4], linked to the local variation in the storm power index of Dolan and Davis [27]. Thus, the intensity of storm waves depends on several factors, mainly the wave heights and wave period during the storm, the persistence of storms, and the direction of storm waves with respect to the shoreline. An assessment of these parameters that characterize storm waves occurred over a considerable period of time will provide a better understanding of the storm regime and allow for a better assessment of the likely intensities of a storm wave along the coast.

In the present study, we aim to evaluate the trend in storm wave intensity based on total storm wave energy of each storm event (*TSWE*), also called energy flux and computed

following Molina et al. [28], and on the storm power index (*SPI*), derived by Dolan and Davis [27], calculated for each characterized storm. The *SPI* index is applied by several researchers in the evaluation of the impacts of storms in the coastal zones [5,29–32]. These studies showed a significant correlation between the storm power index [27] and the storm's causality. For our aim, the storm wave events occurred in the whole western Mediterranean Sea basin during the last 41 years were characterized according to the definition adopted by Ojeda et al. [33], which characterizes a storm as an event during which significant wave heights exceed a minimum threshold H_s for a minimum period of 12 h. Thus, the storm threshold height is defined according to the wave climate data of each grid point of the western Mediterranean based on the formula proposed by Birkemeier et al. [34] and used by Walker and Besco [35] and Mendoza et al. [36].

Trend analysis was based on the Theil–Sen slope estimator and the Mann–Kendall test to assess the significance of trends with several levels of confidence. Spatial assessment of storm wave intensity trends helps to assess the influence of global warming and global change on storm regimes in the Western Mediterranean basin and helps to define the areas most affected by climate change hazards. Thus, the database and the results developed during this study will constitute a decision-making tool that should be considered to ensure a more sustainable development of maritime activities carried out in areas experiencing significant trends in storm wave intensity.

2. Methodology

Increases in storm intensity and wave heights constitute an important factor to be considered in the assessment of global climate change and coastal hazards [25]. For the Mediterranean climate, several observable physical changes are experiencing trends that may extend into the future [16,37]. Increasing trends in storm intensity resulting from global climate variations may increase coastal vulnerability, risk in maritime transport, risk in offshore activities, and affect sustainable development on the Western Mediterranean coasts. Increased storms accompanied by a temporary rise in local sea level [38] will allow energetic storm surges to reach higher beach and dune areas, which can lead to severe erosion [39].

During this study, trends in storm wave intensities are assessed in three main steps. Taking into account one grid point every 0.198°, extracted from a validated wave hindcast of 0.033° resolution (Section 2.1), the first step consists of characterizing the storm wave events occurring in the western Mediterranean Sea during the last 41 years. These storms are characterized by their persistence, their average direction, and the variations in significant wave heights during the storm. The second step consists of the calculation of two main parameters used to determine the storm's intensity. These two parameters are the storm intensity index of Dolan and Davis [27] and the total wave energy during each storm calculated according to [28] as detailed below. The final step is the analysis of annual trends in storm wave energies and *SPI* storm power index. For this analysis, the Theil–Sen slope estimator was used for the slope estimation and the Mann–Kendall test was used for the assessment of the significant of the storm intensity trends. Details on the analysis method are presented in following subsections.

2.1. Wave Hindcast

During this study, a high-precision hindcast wave dataset was used. This wave hindcast, developed using a SWAN model [40,41], was calibrated specifically for the western Mediterranean Sea [42]. This wave hindcast was developed to carry out a detailed assessment of the wave energies resources in the Algerian coast [43], and it is updated annually using the same model, the same numerical and physical parameters, and the same spatial and temporal resolution of 0.033° and 3 h, respectively.

The CFSR (Climate Forecast System Reanalysis) wind [44,45] was used for forcing the wave model. This reanalysis was developed and provided by the National Centers for Environmental Prediction (NCEP) from the webservices https://rda.ucar.edu/. CFSR data are characterized by a very high temporal resolution of 1 h, considered to be necessary in the estimation of storm peaks [46], and covers 41 years. The CFSR's accuracy was approved in several studies with a slight overestimation of wind speed [47–53]. For an efficient study of coastal hazards, a slight overestimation of wind speed and significant wave heights can be preferred than a slight underestimation to ensure sustainable development and an improved security.

Using the CFSR wind field [44,45], the model was run in the third generation and in nonstationary mode using the STOPC (Stop Criterion) convergence criterion requiring 99% of the active grid points to be converged across the entire western Mediterranean Domain from 17° E to 6° W and from 35° N to 45° N. The selected time step was 30 min with a maximum of 4 iterations per time step, and the directional wave energy density spectrum function was discretized using 36 directional bins and 35 frequency bins between 0.033 Hz and 1.0 Hz. For the boundary condition, the southeastern and western boundary of the computational grid was defined with the JONSWAP spectrum with a peak enhancement parameter gamma = 3.3. Further information on the wave model setup are detailed in Amarouche et al. [42], and some physical computation settings are summarized in Table 1.

Table 1. The calibrated physical processes' settings of SWAN model used for the development of the wave hindcast database [42].

Physical Process	Formula References	Parameters
Linear wind growth	[54]	
Exponential wind growth	[55]	
Whitecapping	[56,57]	$C_{ds2} = 1.0$ & delta = 1
Quadruplets wave–wave interactions	the discrete Interaction approximation (DIA) [58]	$\lambda = 0.25$ & $C_{n/4} = 3.0 \times 10^7$
Triads wave–wave interactions	[59]	$\alpha_{EB} = 0.1$
Depth-induced breaking	[60]	$\alpha_{BJ} = 1.0$ & $\gamma_{BJ} = 0.73$
Bottom friction	[61]	$C_{FJON} = 0.038$

For the evaluation of the wave hindcast accuracy, validation was carried out based on 11 wave buoys. The results were detailed in Amarouche et al. [42,43]. In Table 2, we presented same statistical errors obtained by comparing the hindcast wave data against wave measurements of 11 buoys around the western Mediterranean sea. The results show a good accuracy of the wave hindcast, with average scatter index of 0.298 and 0.194 for both significant wave height (H_s) and zero crossing wave period (T_{m02}), respectively. Thus, a high correlation is recorded in all buoys, with an average of 0.925 and 0.83 for H_s and T_{m02}, respectively, reflecting the high precision of the calibrated SWAN model used during this study. Further detail on the SWAN model calibration and accuracy assessment can be found in Amarouche et al. [42].

Table 2. Statistical error results obtained during the validation of SWAN coarse grid model [42,43].

Buoy Name/Positions	Used Period	Nbr of Observation	SI		Bias		R	
			H_s	T_{m02}	H_s	T_{m02}	H_s	T_{m02}
Matifou 3.22° E 36.84° N	1 October 1998 to 31 March 1999	1304	0.3	0.15	0.15	0.17	0.92	0.88
Azzefoun 4.39° E 36.917° N	1 September 2000 to 28 February 2001	1196	0.31	0.21	0.09	−0.03	0.92	0.78
Kala 8.43° E 36.92° N	1 January 2002 to 31 December 2002	2480	0.3	0.18	0.01	−0.43	0.93	0.89
Palos −0.33° E 37.65° N	1 January 2007 to 31 December 2009	25,470	0.30	0.14	0.15	−0.07	0.92	0.82
Dragonera 2.1° E 39.55° N	1 January 2007 to 31 December 2009	25,222	0.30	0.18	0.05	−0.45	0.92	0.84
Tarragona 1.47° E 40.68° N	1 January 2008 to 31 December 2008	8717	0.30	0.17	0.03	−0.35	0.91	0.86
Buger 3.65° E 41.92° N	1 January 2008 to 31 December 2008	6374	0.27	0.18	−0.04	−0.48	0.94	0.88
Mahon 4.42° E 39.71°N	1 January 2007 to 31 December 2009	23,257	0.29	0.15	0.16	−0.30	0.94	0.88
Nice 7.23° E 43.63° N	1 January 2008 to 31 December 2008	8177	0.38	0.27	−0.02	−0.76	0.87	0.63
Porquerolles 6.20° E 42.97° N	1 January 2000 to 31 December 2000	3129	0.25	0.17	−0.03	−0.4	0.94	0.88
Marseille 3.66° E 43.33° N	1 January 2000 to 31 December 2000	2095	0.28	0.29	−0.06	−0.92	0.96	0.84

2.2. Storm Wave Characterization

A storm wave is a climate event defined as a time period during which the significant wave height exceeds a minimum threshold H_s during a considerable time lapse. The storm wave events identified during the present study are characterized according to the definition established by [33], who considered a storm wave as an event where the observed significant wave heights exceed a threshold height for at least 12 h, whereas the $H_{s,\ threshold}$ is calculated according to the long term wave climate data in the concerned area according to Birkemeier et al. [34] and Walker and Besco [35], which defines $H_{s,\ threshold}$ for each study area as the long-term mean of significant wave heights $\overline{X}$ plus twice the standard deviation according to the following formula:

$$H_{s,\ threshold} = \overline{X} + 2\,\sigma \tag{1}$$

Figure 1 shows the threshold heights calculated based on this formula for all the grid points evaluated during the present study. This figure clearly shows a variation in the threshold heights to be considered in each zone and their dependence on the local wave climate, which is related in turn to the depth and proximity of the coast. Thus, in order to ensure that the event is statistically independent [33], two consecutive storm waves are considered independent if the significant wave heights between two events remain above $H_{s,\ threshold}$ for a minimum of 48 h; this separation period allows a distinction of macro-meteorological phenomena [62]. The total storm number characterized based on these criteria are mapped.
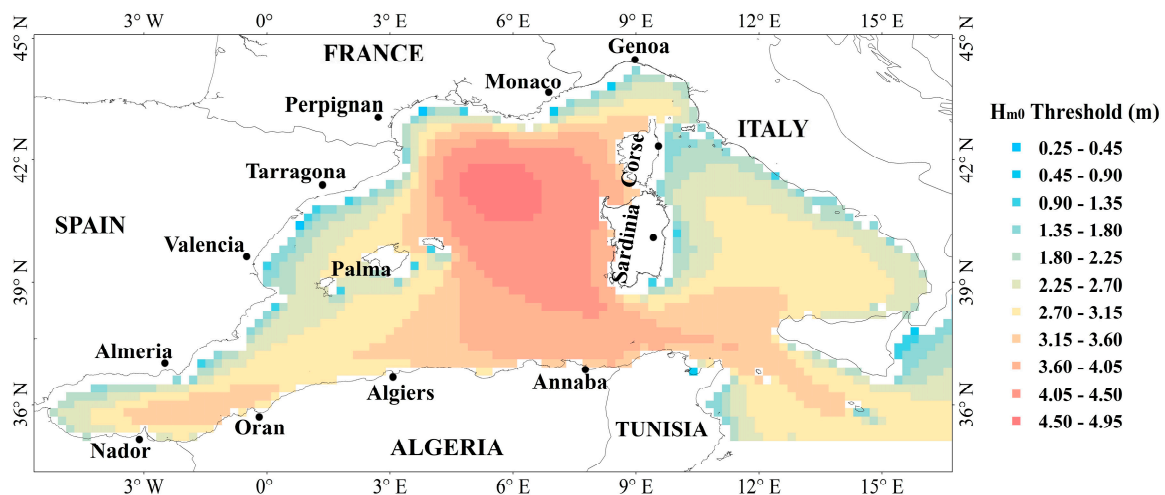
Figure 1. Significant wave height thresholds used for the characterization of storm wave events.

Figure 2 illustrates three independent consecutive storms that are characterized based on the definition of [33] in the time series plot of significant wave heights; thus, on the same figure the total energy of each storm wave is illustrated by a green area above the time series plot of wave powers (P_w) between the starting time t_0 of the storm and the ending time t_n. This area is mathematically represented by the following integral:

$$TSWE = \int_{t_0}^{t_n} P_W(t) \, dt \tag{2}$$

where TSWE represents the total energy during the storm wave and P_w is the wave energy flux (wave power) approximated by the following formula

$$P_W = \frac{\rho g^2}{64\pi} \times H_S^2 \times T_e \ldots \tag{3}$$

where T_e is the energy period defined in terms of spectral moments, H_s is the significant wave height, and ρ is the seawater density taken as 1027 kg/m^3. The wave parameters (H_s and T_e) used for the calculation of the wave power P_w were both obtained from the same wave hindcast database developed using the SWAN model. This simple definition of TSWE based on the total wave power during the storm period is adopted and illustrated by Molina et al. [28] and can be used to quantitatively evaluate and classify storm waves in terms of their intensities.

In addition to the TSWE, the storm power index [27] was computed for each storm event and was also used for the evaluation of storm intensity trends in the Mediterranean Sea. The SPI is determined only from the mean significant wave heights during the storm and the persistence of the storm as follows:

$$SPI = H_s^2 \times T_d \tag{4}$$

where T_d is the storm duration in hours. The several studies [29,30,36,50,63–66] have shown a strong correlation between the *SPI* and the damage recorded in coastal areas. As such an evaluation of the annual trend in the *SPI* is considered valuable to assess the annual trend in the *SPI* as an indicator of storm intensity trends. The storm intensity trend is thus evaluated in terms of both *TSWE* and *SPI*.
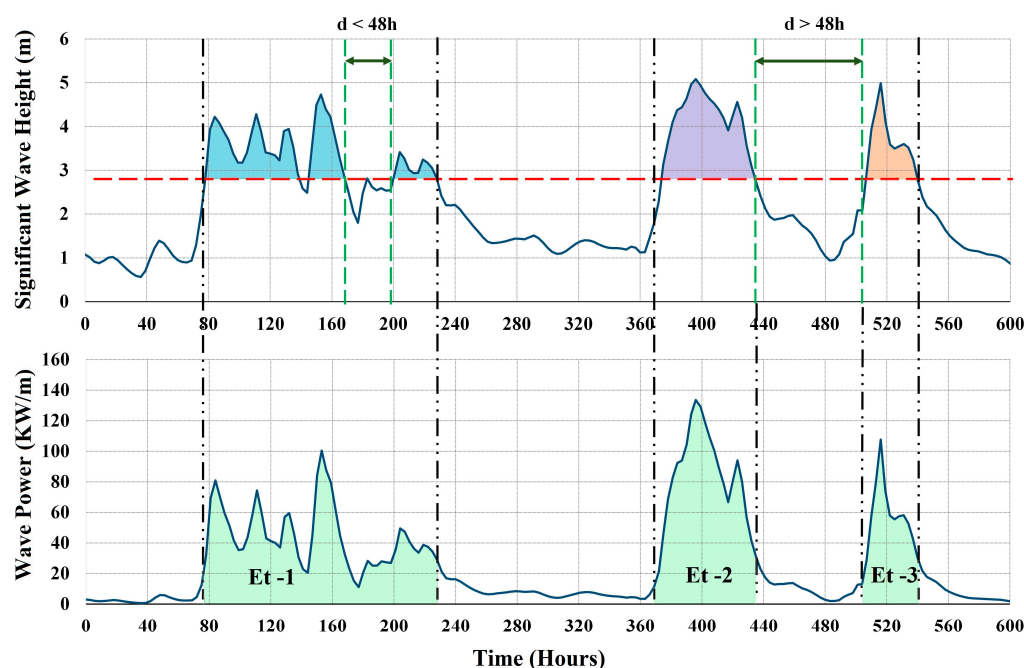
Figure 2. Time series plot illustrating three storm waves (distinguished by colors) characterized for a significant wave height threshold of 2.7 m with a minimum interval between two consecutive storms of 48 h.

2.3. Trend Aanalysis Method

Currently, the combined approach of Theil–Sen slope estimator [67,68] and Mann–Kendall test [69,70] is one of the most commonly practiced methods in the analysis of wave and wind climate trends [71–77]. The Theil–Sen slope estimator was adopted by Theil [68] and reviewed by [67] by considering the asymptotic properties of the estimators. This method does not require that constant values should be all distinct, and it is based on weaker assumptions [67]. Furthermore, the Theil–Sen estimator is not sensitive to the non-normality. Therefore, this method is more suitable for the analysis of the wave climate trend. The statistical approach of this method consists of determining the slopes a_{ij} between the set of values distributed as a function of time, two by two, by considering all possible pairs using the following formula:

$$a_{ij} = \frac{(Y_j - Y_i)}{(t_j - t_i)} \qquad with \ \ 1 < i < j < n \tag{5}$$

where Y is the annual average data and t is the year, n is the total observations, and i and j are indexes that point out the position of all the pair of observations points used for the slope estimation. Then, the non-parametric Theil–Sen slope is determined as the median value of all pair's points slope a_{ij}.

For the evaluation of the trend significant in storm intensity, the non-parametric test of Kendall was used. This test was developed and initiated by Mann [70] and illustrated statistically by Kendall [69]. For the application of the Mann–Kendall test, the normality distribution of the evaluated data is also not required. The Mann–Kendall test hypothesis are H_0 (null hypothesis), in which we assume that the trend over the time is not existing or nonsignificant, and H_1 (alternative hypothesis), in which we assume an increasing or decreasing trend over time and that this trend is significant.

Practically, the Mann–Kendall test can be summarized in four steps. The first step is preparing and ordering the data chronologically. To study the annual (mean and max) trends in TSWE and SPI over 41 years, the total observation n is 41 and the annual observations (Y_i) (mean and max) of each parameter was chronologically ordered $Y_i \ldots Y_n$. The second step of the test is the calculation of the total n(n − 1)/2 possible difference $y_j - y_i$;

where *i*-values indicate the order of the years of observation; $i = 1 \ldots n - 1$, and $j = i + 1 \ldots n$. In the third step, the signs of the possible difference set $Y_j - Y_i$ are to be used to calculate The Mann–Kendall test statistic *S* as follows:

$$S = \sum_i^{n-1} \sum_j^{n} sgn\left(Y_j - Y_i\right) \tag{6}$$

The signs of the differences $y_j - y_i$ are used to calculate the Mann–Kendall test statistic *S* using the following formula $\sum_i^{n-1} \sum_j^{n} sgn\left(Y_j - Y_i\right)$, where $sgn(y_j - y_i)$ is an indicator function defined on the basis of three criteria:

$$\begin{aligned} sgn(Y_j - Y_k) &= 1 \text{ if } Y_j - Y_k > 0 \\ sgn(Y_j - Y_k) &= 0 \text{ if } Y_j - Y_k = 0 \\ sgn(Y_j - Y_k) &= -1 \text{ if } Y_j - Y_k < 0 \end{aligned} \tag{7}$$

The fourth step is to compute the standardized *S* statistic "*Z*" following [67] description.

$$Z = \begin{cases} \frac{S-1}{\sqrt{Var(S)}} & if \ S > 0 \\ 0 & if \ S = 0 \\ \frac{S+1}{\sqrt{Var(S)}} & if \ S < 0 \end{cases} \tag{8}$$

where *Var(S)* is computed according the following

$$Var(S) = \frac{1}{18} \left[n(n-1)(2n+5) - \sum_{i=1}^{m} T_i(T_i - 1)(2T_i + 5) \right] \tag{9}$$

where *m* is the number of related values in the time series, whereas T_i is the number of data values in the mth group up to observation *i*.

Finally, the last step is the test of the null hypothesis (H_0) by comparing the test statistic *Z* absolute computed value against the theorical $Z_{1-\alpha/2}$ obtained from the standard normal table. This test was evaluated by considering different significance levels α of 0.01, 0.05, 0.1, and 0.2. H_0 is rejected if $|Z| > Z_{1-\alpha/2}$, and that means that there is a significant trend for a confidence level of $1 - \alpha$, and the trend direction is defined as increasing or decreasing depending on the *Z* value sign.

3. Results and Discussion

Based on the storm criteria detailed in Section 2.2, the storm wave events occurring across the whole western Mediterranean Sea were characterized according to the significant wave heights and their duration. The number of storms occurring during the last 41 years was computed spatially every 20 km from the initial wave hindcast grid of 3 km of resolution (the exact point value of the grid was mapped without interpolation). Figure 3 illustrates the number of storm events recorded during these last four decades. This result shows a considerable spatial variation in the distribution of the number of wave storm events, which mostly varied from 400 to 690 events, corresponding to around 10 to 16 events per year. The average annual number of storm events is almost in accordance with the results of Martzikos et al. [78], although the methodologies used for the storm wave characteristics are different. The area that has experienced the higher storm event numbers during the last four decades is located above the latitude 40, an area also characterized by a high probability of the Medicane (Mediterranean tropical-like cyclone) development [79], and also in the Eastern part of the Alboran Sea (S1). By comparing the spatial distribution of storms (Figure 3) with the long-term annual mean and maxima of wave energy and H_s presented in [42], we observe a significant difference in the spatial distribution between these three parameters. This difference may depend on the variability of wave climate

in each region and implies that the number of storms is not directly dependent on the long-term annual mean and/or annual maxima of significant wave height and wave energy. The western Mediterranean basin is often exposed to different strong winds: the Vendaval wind from South West of the Balearic basin, the Ponente wind from the West through the Straits of Gibraltar, the Mistral wind from the northwest, the Sirocco wind from the south and southeast, the Levant wind from east and northeast, the Libeccio wind from southwest in Corsica and the Tyrrhenian basin, the Tramontane wind from the north, and the Marin from the southwest Gulf of Lion.

Figure 3. Map showing the number of storm wave events occurring at each analyzed point during the period of 1979 to 2019.

All the storm occurring in each point, was considered in the computation of the annual mean of the TSWE and the storm power index, was used for the annual trend's analysis and the result was mapped by considering the real grid point without interpolation. In the present study, the storm intensity was evaluated in terms of the total energy during each storm events and in terms of the storm power index [27].

The annual trends of these parameters shown in Figures 4–7 are used as indicators of storm wave intensity trends, given that there is no defined and specific parameter quantifying the storm wave intensity. Trends in maximum and mean TSWE and SPI were assessed. The results show a strong spatial correspondence between the area experiencing a significant trend in maximum storm intensity and the area experiencing a significant trend in mean storm intensity. Figures 4–7 illustrate the areas experiencing a significant annual trend in TSWE and SPI (mean and maximum) according to Mann–Kendall test results as well as the estimated slope values for each area based on the Theil–Sen slope estimator. These results show that a very important part of the western Mediterranean Sea basin has experienced an increasing slope and a considerable area has experienced a significant increase in the *TSWE* with a confidence level >95%. This area is principally located in five different parts. The first part is located in the east of the Alboran Sea, where a significant trend in storm intensity is estimated with a slope >32 kWh·m^{-1}·year^{-1} and >100 kWh·m^{-1}. year^{-1}, respectively, for annual average and maximum of *TSWE* and a slope >6 kWh·m^{-1}. year^{-1} and >28 kWh·m^{-1}. year^{-1} for annual average and maximum of *SPI*, respectively. The second part is the eastern Algerian basin, where a significant increase in both *SPI* and *TSWE* was recorded with a confidence level >95% and a very steep slope for both the annual average *SPI* and annual average *TSWE* of > 6 m^2·h·year^{-1} and >32 kWh·m^{-1}·year^{-1}, respectively. Thus, a very steep slope has been estimated for annual maximum *SPI* and annual maximum *TSWE* of >28 m^2·h·year^{-1} and >120 kWh·m^{-1}·year^{-1}, respectively.

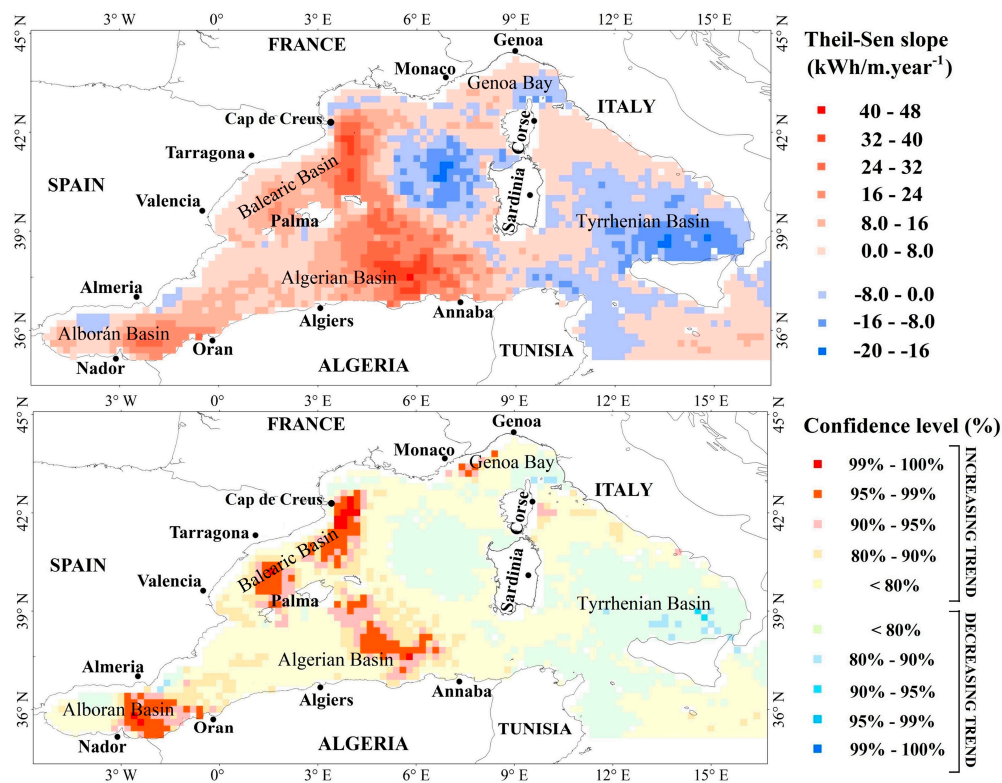**Figure 4.** Spatial distribution of long-term trends (Theil–Sen slope in kWh·m^{-1}·year^{-1}) of the annual average of the total storm wave energy (*TSWE*) (**upper panel**) and their significant trends according to the Mann–Kendall test at different confidence levels (**lower panel**).
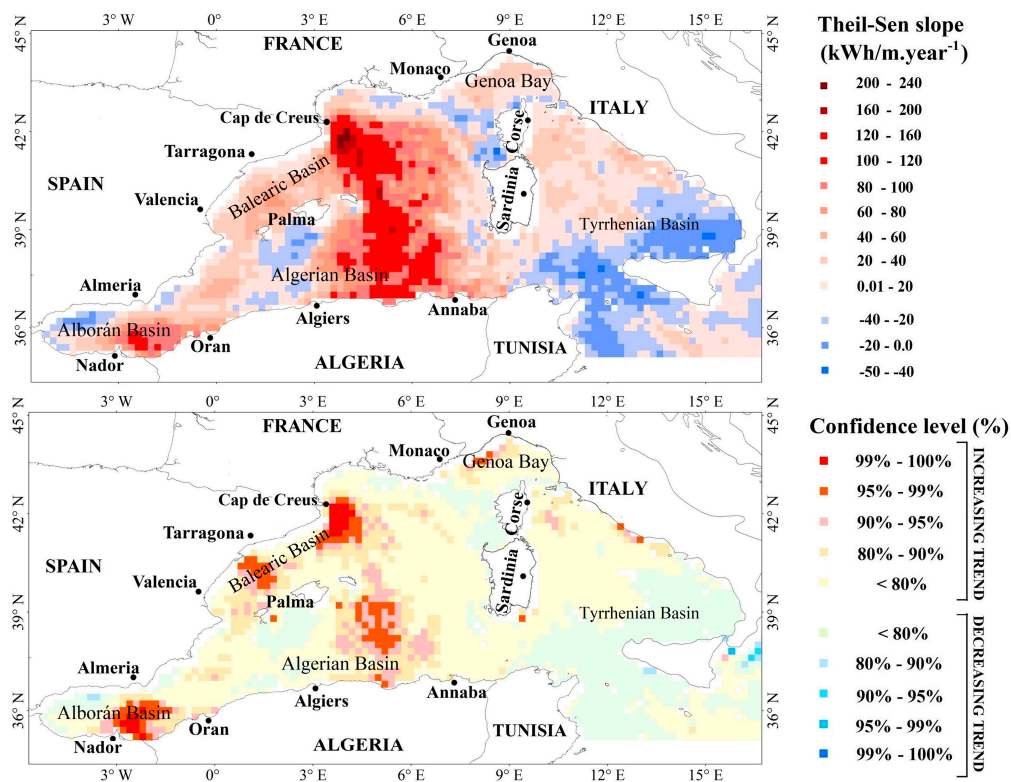

Figure 5. Spatial distribution of long-term trends (Theil–Sen slope in kWh·m^{-1}·year^{-1}) of the annual maxima of the total storm wave energy (TSWE) (**upper panel**) and their significant trends according to the Mann–Kendall test at different confidence levels (**lower panel**).
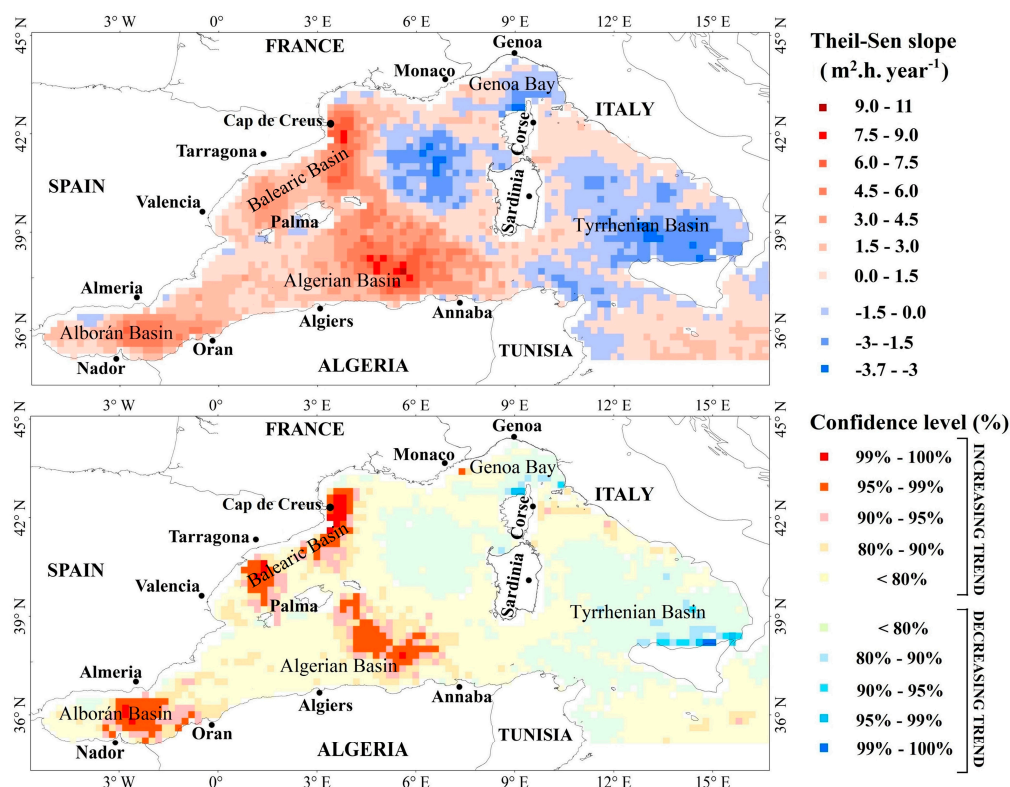
Figure 6. Spatial distribution of long-term trends (Theil-Sen slope in m²·h·year⁻¹) of the annual average of Storm Power Index (*SPI*) (**upper panel**) and their significant trends according to the Mann Kendall test at different confidence levels (**lower panel**).

Figure 7. Spatial distribution of long-term trends (Theil–Sen slope in m²·h. year⁻¹) of the annual maxima of the Storm Power Index (*SPI*) (**upper panel**) and their significant trends according to the Mann–Kendall test at different confidence levels (**lower panel**).
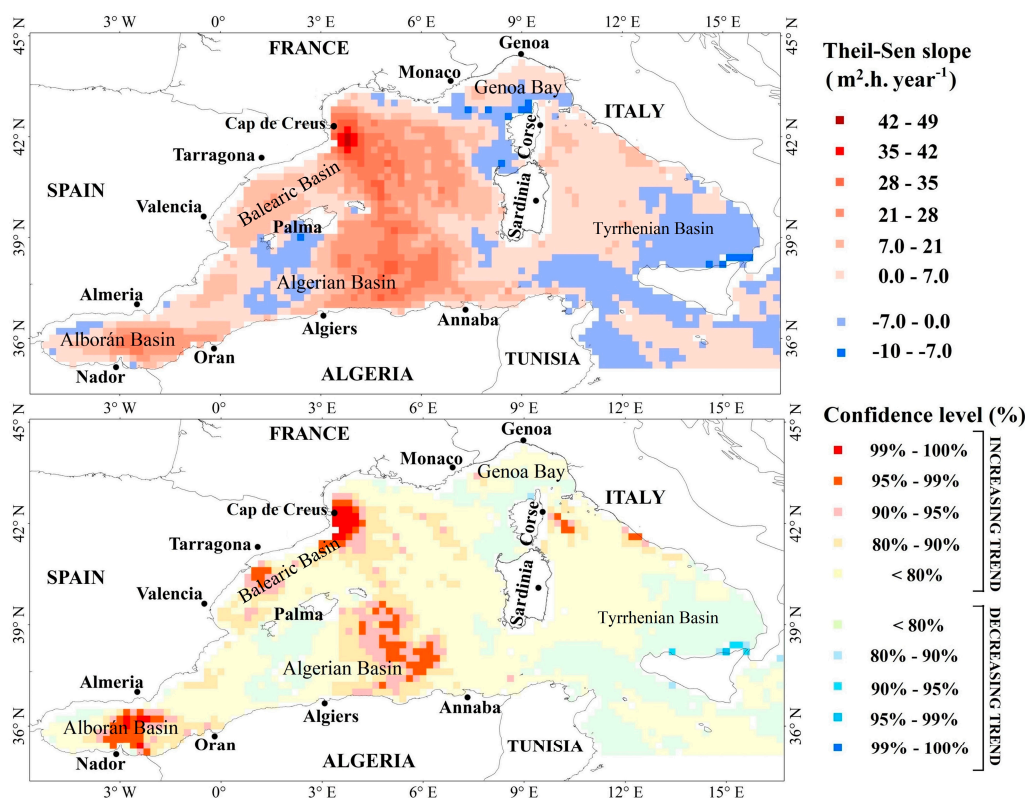
The third area, is located in western part of Genoa coast, where a significant trend is estimated for max and average *TSWE* with a confidence level exceeding 95% and a slope >8 kWh·m^{-1}·year^{-1} for the average *TSWE* and >40 kWh·m^{-1}·year^{-1} for max *TSWE*. In the same area, a significant trend was also recorded for the SPI but with a lower confidence level, and only in one grid point significant trend was detected with a 95% confidence level. This can be explained by an influence of wave period variation and trend, which is considered only in the wave *TSWE* formulation. The fourth interesting area is located off Cap de Creus in the western part of the Gulf of Lion, where the significant trend is estimated with a confidence level >99% for both *SPI* and *TSWE*. The slope value estimated in this area exceeds 6 m^2·h·year^{-1} and 32 kWh·m^{-1}·year^{-1} for the annual average of *SPI* and *TSWE*, respectively, and exceed 42 m^2·h·year^{-1} and 200 kWh·m^{-1}·year^{-1} for the annual maximum of *SPI* and *TSWE*, respectively. The last area that experienced a significant trend in storm intensity is located off the coast of Tarragona and covers a considerable area of the Balearic on which a significant trend in both annual average and maximum of the *TSWE* and *SPI* are estimated with a confidence level exceeding 95% and with a slope of 6 m^2·h·year^{-1} and 16 kWh·m^{-1}·year^{-1} for average *SPI* and *TSWE* and 21 m^2·h·year^{-1} and 40 kWh·m^{-1}·year^{-1} for maximum *SPI* and *TSWE*, respectively. This part of the Balearic sea as well as the eastern part of Gulf of Lion experienced an extreme catastrophe in January 2020 (Storm Gloria) during which new records were recorded by the wave buoy measurements of Tarragona and Valencia, causing catastrophe damage along the French and Spanish coasts [12]. Knowing that the results obtained during this study are elaborated based on wave climate data from 1979 to 2019, we can note that the results obtained by this analysis allowed us to estimate the increase in the intensity of storm waves in the affected area during Storm Gloria 2020 [12]. However, other catastrophic storms may probably occur in the coming years and in all areas characterized by a very significant trend. Consideration of trends in storm wave intensities in the prediction of areas with high risks and in the future planning on sustainable development can therefore provide significant guidance.

For a better visualization, a time series plot indicating the annual variation of TSWE and SPI was presented for five different stations located in the areas experiencing an increasing trend in TSWE and SPI (presented in Figure 3); the time series plots are presented in Figures 8 and 9 and details on the geographical location and estimated slope in these five stations are presented in Table 3. The plots illustrate clearly the annual variation and the increasing trend in both *SPI* and *TSWE* for the annual average and maximum. Thus, these plots show a strong correspondence between the trends in mean storm intensity and trends in the most violent annual storm waves; this information may reveal that the assessed trends are not only due to exceptional annual events but to a deeper change and trend in the storm pattern observed during the year, and these areas may therefore experience strong climate change.

Table 3. Geographic information and estimated slopes of SPI and TSWE in five selected stations.

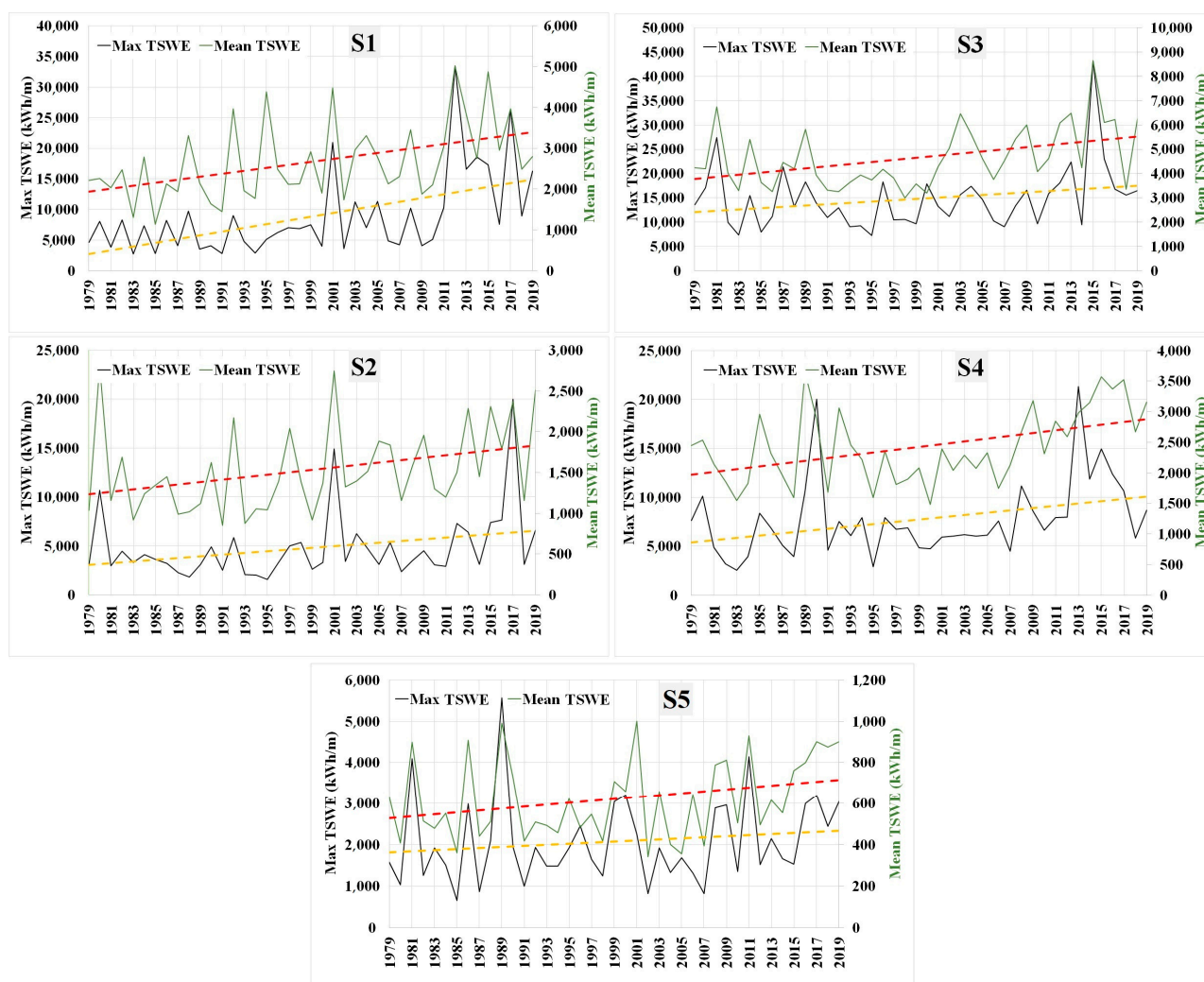| Stations.	Lon.	Lat.	Depth (m)	Distance from the Coast (km)	Estimated Annual Slope of Mean SPI (m^2·h·year^{-1})	Estimated Annual Slope of Mean TSWE (kWh·m^{-1}·year^{-1})	Estimated Annual Slope of Max SPI (m^2·h·year^{-1})	Estimated Annual Slope of Max TSWE (kWh·m^{-1}·year^{-1})
S1	2.6° W	35.8° N	750	51	5.9	26.1	23.2	114.8
S2	1.4° E	40° N	1439	88	3.3	14.2	14.1	57.2
S3	3.6° E	41.8° N	1326	35	6.4	26.5	37.4	149.7
S4	5.8° E	37.6° N	2812	74	5.7	40.8	21.7	98.5
S5	7.6° E	43.4° N	2418	44	2.1	5.9	7.5	18.5

Figure 8. Time series plots of annual average and maximum *TSWE* between 1979 and 2019 in five different locations of the Mediterranean Sea that have experienced the significant trend during this period. The dashed line shows the linear trend of each time series. The discontinued line illustrates the estimated Theil–Sen slope adjusted to the corresponding time series plot.

The present study represents the first attempt to assess the intensity of storm waves according to the TSWE and SPI. The existing studies [19,75–77,80–85] are focused on the evaluation of individual significant wave height trends and wind speed trends on which the storm wave events are highly dependent. Compared to the global study on wind and wave trend analysis, the result obtained during this study are in the line with the trend results of the 90th and 99th percentile significant wave height and wind speed obtained by [19,80]. Thus, a study on significant wave height trends recently made by Timmermans et al. [81] shows a strong and significant increasing trend in significant wave height in the western part of the Mediterranean basin for several analyses of wave data sources. Timmermans et al. [81] results show that the Mediterranean basin experiences one of the higher positives slope around the world during the period of 1992–2017. Thus, in comparing the area experiencing a significant increase in storm intensity with the area experiencing a significant increase in the maximum Hs as defined by De Leo et al. [74], we can notice an intersecting correspondence along the western European coast but not along the African coast. The area characterized by a significant increasing trend in storm intensity covers a more important space. This difference can be a fact of the trend in storm duration, which can considerably affect storm intensity. Results obtained are also in agreement with the results obtained by Molina et al. [28], which show an increase in the

intensity of storm waves in the eastern Alboran basin between 1979 and 2014, and with the results of Jiménez [4], which show an increase in the intensity of storms on the Catalan coast for the period of 1958–2008. The results obtained in the present study and in the above-mentioned studies are based exclusively on the trends of the SPI and the TWSE by considering the overall storm wave events. However, consideration of storm direction can provide more detailed information on the main climatic events causing the trends in storm wave intensity. Table 4 illustrates the occurrence of storms by direction in the five selected hotspots. Western storm waves are very dominant in the Alboran Basin, these storms can be generated by strong Vendaval and Ponente winds, and a trend in storm intensity in this area can be affected by the Atlantic climate. The storms that occur in the Balearic Basin mainly originate from the north and northeast and can be linked to the Mistral, the Tramontane, and probably the Levantine wind. In the station S3, located off Cap de Creus in the western part of the Gulf of Lion, the dominant storm waves are from northward and can be linked to the Mistral and Tramontane. In the southern hotspot S4, the storm wave directions are practically north and west and can also be related to the Mistral, Tramontane, Vendaval, and Ponente winds. For the S5 hotspot located off of Monaco, we observe a domination of storm wave events from the southwest, probably related to the Libeccio storm winds. The storm wave events can also originate by exceptional storm events, such as Storm Gloria and other medicane events.
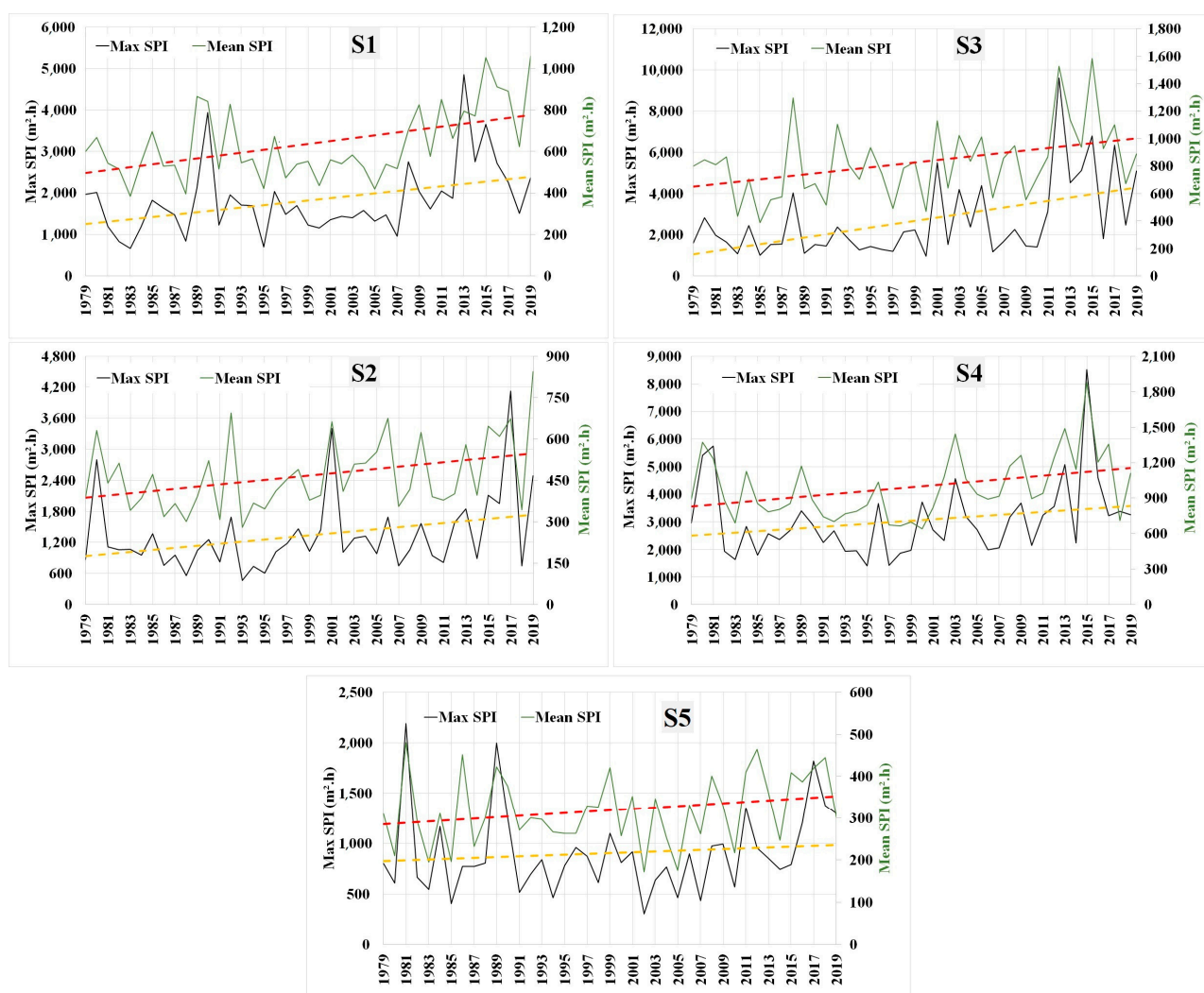

Figure 9. Time series plots of annual average and maximum *SPI* between 1979 and 2019 in five different locations of the Mediterranean Sea that have experienced the significant trend during this period. The dashed line shows the linear trend of each time series. The discontinued line illustrates the estimated Theil–Sen slope adjusted to the corresponding time series plot.

Table 4. Number of storm wave events per direction in the five selected stations.

Stations:	S1	S2	S3	S4	S5
N	10	107	348	167	1
NE	187	166	40	7	102
E	0	28	65	20	78
SE	0	7	10	0	10
S	0	11	6	0	28
SW	0	70	23	0	347
W	323	34	0	148	4
NW	11	84	7	148	0

4. Conclusions

All storm wave events occurring in the western Mediterranean Sea over the last 41 years were characterized one by one, and the *SPI* and *TSWE* were determined for each storm event and in each grid point. Based on the Theil–Sen slope estimator and the Mann–Kendall test, the annual trend of the maximum and average of the *SPI* and *TSWE* were determined for the entire western Mediterranean Sea. The results allowed us to determine the trend slope of the *SPI* and *TSWE* and to identify the areas characterized by a significant increasing trend with an acceptable confidence level. According to the results, a very large part of the western Mediterranean Sea shows an annual increasing trend in *SPI* and *TSWE*, both in maximum and average, which is in line with the results of Young et al. [80], Young and Ribal [19], and Timmermans et al. [81]. Five areas are defined as hotspots, with a significant increasing trend and a confidence level above 95%. These areas are the East Albert Sea, the eastern Algerian Basin, the West Genoa coast, off of Cap de Creus, and off the coast of Tarragona. These last two areas were recently exposed to a record storm in January 2020 (Storm Gloria), which caused heavy damage on the French and Spanish coasts [12]. According to the present findings, a considerable and very probable risk can be expected in this area, and more intensive storms are likely to occur in the coming years.

The area that experienced a significant trend in storm intensity based on the *SPI* and *TSWE* are considerably larger than the area that experienced a significant trend in significant wave height determined by De Leo et al. [74] for the western Mediterranean basin. This can be explained by a significant influence of the storm duration trends. In order to ensure a sustainable development of the coasts and offshore in these hazardous areas, it is strongly recommended to take into account the results presented on the storm intensity trend with a detailed analysis of the wave climate variation in order to support decision-making as well as for risk assessment and management. Thus, a consideration of the wave direction during storm events can provide advantageous knowledge about the storm wave regime in the hotspot area. Our perspective is to develop a more detailed study in the selected hotspots, by considering the storm waves' direction to assess the likely effect of the detected change in storm wave climates on the coastal zone and for the location of the most affected coasts by the increasing trend in storm wave intensity.

Author Contributions: Conceptualization, K.A. and A.A.; methodology, K.A. and A.A.; software, K.A.; validation, K.A.; formal analysis, K.A.; resources, K.A and A.A.; data curation, K.A. and A.A.; writing—original draft preparation, K.A.; writing—review and editing, K.A. and A.A. All authors have read and agreed to the published version of the manuscript.

Conflicts of Interest: The authors declare no conflict of interest.

References

1. Jackson, D.; Drumm, A.; McEvoy, S.; Jensen, Ø.; Mendiola, D.; Gabiña, G.; Borg, J.A.; Papageorgiou, N.; Karakassis, Y.; Black, K.D. A pan-European valuation of the extent, causes and cost of escape events from sea cage fish farming. *Aquaculture* **2015**, *436*, 21–26. [CrossRef]
2. Zhang, Z.; Li, X.-M. Global ship accidents and ocean swell-related sea states. *Hazards Earth Syst. Sci.* **2017**, *17*. [CrossRef]
3. Xu, S.; Ma, M.; Yin, K.; Tang, S. Risk evaluation system of navigation security based on coupled wind and wave model: A case of study of Qiongzhou strait. *IET Intell. Transp. Syst.* **2020**, *14*, 1311–1318. [CrossRef]
4. Jiménez, J.A.; Sancho-García, A.; Bosom, E.; Valdemoro, H.I.; Guillén, J. Storm-induced damages along the Catalan coast (NW Mediterranean) during the period 1958–2008. *Geomorphology* **2012**, *143–144*, 24–33. [CrossRef]
5. Amarouche, K.; Akpınar, A.; Çakmak, R.E.; Houma, F.; Bachari, N.E.I. Assessment of storm events along the Algiers coast and their potential impacts. *Ocean Eng.* **2020**, *210*, 107432. [CrossRef]
6. Marzeddu, A.; Oliveira, T.C.A.; Sánchez-Arcilla, A.; Gironella, X. Effect of wave storm representation on damage measurements of breakwaters. *Ocean Eng.* **2020**, *200*, 107082. [CrossRef]
7. Casas-Prat, M.; Sierra, J.P. Trend analysis of wave storminess: Wave direction and its impact on harbour agitation. *Nat. Hazards Earth Syst. Sci.* **2010**, *10*, 2327–2340. [CrossRef]
8. Wang, Y.C.; Wang, Y.Z.; Hong, N.N. Dynamic stability analysis of caisson breakwater in lifetime considering the annual frequency of severe storm. *China Ocean Eng.* **2015**, *29*, 287–300. [CrossRef]
9. Sanuy, M.; Jiménez, J.A. Sensitivity of Storm-Induced Hazards in a Highly Curvilinear Coastline to Changing Storm Directions. The Tordera Delta Case (NW Mediterranean). *Water* **2019**, *11*, 747. [CrossRef]
10. Sanuy, M.; Duo, E.; Jäger, W.S.; Ciavola, P.; Jiménez, J.A. Linking source with consequences of coastal storm impacts for climate change and risk reduction scenarios for Mediterranean sandy beaches. *Nat. Hazards Earth Syst. Sci.* **2018**, *18*, 1825–1847. [CrossRef]
11. Lira-Loarca, A.; Cobos, M.; Losada, M.Á.; Baquerizo, A. Storm characterization and simulation for damage evolution models of maritime structures. *Coast. Eng.* **2020**, *156*, 103620. [CrossRef]
12. Amores, A.; Marcos, M.; Carrió, D.S.; Gómez-Pujol, L. Coastal impacts of Storm Gloria (January 2020) over the north-western Mediterranean. *Nat. Hazards Earth Syst. Sci.* **2020**, *20*, 1955–1968. [CrossRef]
13. Cavaleri, L.; Bajo, M.; Barbariol, F.; Bastianini, M.; Benetazzo, A.; Bertotti, L.; Chiggiato, J.; Davolio, S.; Ferrarin, C.; Magnusson, L.; et al. The October 29, 2018 storm in Northern Italy–An exceptional event and its modeling. *Prog. Oceanogr.* **2019**, *178*, 102178. [CrossRef]
14. Sánchez-Arcilla, A.; González-Marco, D.; Doorn, N.; Kortenhaus, A. Extreme values for coastal, estuarine, and riverine environments. *J. Hydraul. Res.* **2008**, *46*, 183–190. [CrossRef]
15. Jiménez, J.A.; Sanuy, M.; Ballesteros, C.; Valdemoro, H.I. The Tordera Delta, a hotspot to storm impacts in the coast northwards of Barcelona (NW Mediterranean). *Coast. Eng.* **2018**, *134*, 148–158. [CrossRef]
16. Cramer, W.; Guiot, J.; Fader, M.; Garrabou, J.; Gattuso, J.-P.; Iglesias, A.; Lange, M.A.; Lionello, P.; Llasat, M.C.; Paz, S.; et al. Climate change and interconnected risks to sustainable development in the Mediterranean. *Nat. Clim. Chang.* **2018**, *8*, 972–980. [CrossRef]
17. Lionello, P.; Scarascia, L. The relation of climate extremes with global warming in the Mediterranean region and its north versus south contrast. *Reg. Environ. Chang.* **2020**, *20*. [CrossRef]
18. Sánchez-Arcilla, A.; González-Marco, D.; Bolaños, R. A review of wave climate and prediction along the Spanish Mediterranean coast. *Nat. Hazards Earth Syst. Sci.* **2008**, *8*, 1217–1228. [CrossRef]
19. Young, I.R.; Ribal, A. Multiplatform evaluation of global trends in wind speed and wave height. *Science* **2019**, *364*, 548–552. [CrossRef]
20. Gulev, S.K. Last century changes in ocean wind wave height from global visual wave data. *Geophys. Res. Lett.* **2004**, *31*, L24302. [CrossRef]
21. Reguero, B.G.; Losada, I.J.; Méndez, F.J. A recent increase in global wave power as a consequence of oceanic warming. *Nat. Commun.* **2019**, *10*, 1–14. [CrossRef]
22. Vieira, F.; Cavalcante, G.; Campos, E. Analysis of wave climate and trends in a semi-enclosed basin (Persian Gulf) using a validated SWAN model. *Ocean Eng.* **2020**, *196*, 106821. [CrossRef]
23. Dobrynin, M.; Murawsky, J.; Yang, S. Evolution of the global wind wave climate in CMIP5 experiments. *Geophys. Res. Lett.* **2012**, *39*. [CrossRef]
24. Meucci, A.; Young, I.R.; Aarnes, O.J.; Breivik, Ø. Comparison of wind speed and wave height trends from twentieth-century models and satellite altimeters. *J. Clim.* **2020**, *33*, 611–624. [CrossRef]
25. Komar, P.D.; Allan, J.C. Increasing hurricane-generated wave heights along the U.S. East Coast and their climate controls. *J. Coast. Res.* **2008**, *24*, 479–488. [CrossRef]
26. Bromirski, P.D.; Kossin, J.P. Increasing hurricane wave power along the U.S. Atlantic and Gulf coasts. *J. Geophys. Res.* **2008**, *113*, C07012. [CrossRef]
27. Dolan, R.; Davis, E. An intensity scale for Atlantic coast northeast storms. *J. Coast. Res.* **1992**, *8*, 840–853.

28. Molina, R.; Manno, G.; Lo Re, C.; Anfuso, G.; Ciraolo, G. Storm Energy Flux Characterization along the Mediterranean Coast of Andalusia (Spain). *Water* **2019**, *11*, 509. [CrossRef]

29. Martzikos, N.; Afentoulis, V.; Tsoukala, V. Storm clustering and classification for the port of Rethymno in Greece. *Water Util. J.* **2018**, *20*, 67–79.

30. Anfuso, G.; Rangel-Buitrago, N.; Cortés-Useche, C.; Iglesias Castillo, B.; Gracia, F.J. Characterization of storm events along the Gulf of Cadiz (eastern central Atlantic Ocean). *Int. J. Climatol.* **2016**, *36*, 3690–3707. [CrossRef]

31. Rangel-Buitrago, N.; Anfuso, G. Coastal storm characterization and morphological impacts on sandy coasts. *Earth Surf. Process. Landforms* **2011**, *36*, 1997–2010. [CrossRef]

32. Rangel-Buitrago, N.; Anfuso, G. An application of Dolan and Davis (1992) classification to coastal storms in SW Spanish littoral. *J. Coast. Res.* **2010**, *64*, 1891–1895.

33. Ojeda, E.; Appendini, C.M.; Mendoza, E.T. Storm-wave trends in Mexican waters of the Gulf of Mexico and Caribbean Sea. *Nat. Hazards Earth Syst. Sci.* **2017**, *17*, 1305–1317. [CrossRef]

34. Birkemeier, W.; Nicholls, R.; Lee, G. *Storms, Storm Groups and Nearshore Morphologic Change, Coastal Sediments' 99*; ASCE Press: Long Island, NY, USA, 1999.

35. Walker, R.A.; Basco, D.R. Application of coastal storm impulse (COSI) parameter to predict coastal erosion. *Coast. Eng. Proc.* **2011**, *1*, 23. [CrossRef]

36. Mendoza, E.T.; Trejo-Rangel, M.A.; Salles, P.; Appendini, C.M.; Lopez-Gonzalez, J.; Torres-Freyermuth, A. Storm characterization and coastal hazards in the Yucatan Peninsula. *J. Coast. Res.* **2013**, *65*, 790–795. [CrossRef]

37. Satta, A.; Puddu, M.; Venturini, S.; Giupponi, C. Assessment of coastal risks to climate change related impacts at the regional scale: The case of the Mediterranean region. *Int. J. Disaster Risk Reduct.* **2017**, *24*, 284–296. [CrossRef]

38. Han, W.; Stammer, D.; Meehl, G.; Hu, A.; Sienz, F.; Zhang, L. Multi-Decadal Trend and Decadal Variability of the Regional Sea Level over the Indian Ocean since the 1960s: Roles of Climate Modes and External Forcing. *Climate* **2018**, *6*, 51. [CrossRef]

39. Zhang, K.; Douglas, B.C.; Leatherman, S.P. Global warming and coastal erosion. *Clim. Change* **2004**, *64*, 41–58. [CrossRef]

40. Booij, N.; Ris, R.C.; Holthuijsen, L.H. A third-generation wave model for coastal regions: 1. Model description and validation. *J. Geophys. Res.* **1999**, *104*, 7649–7666. [CrossRef]

41. Ris, R.C.; Holthuijsen, L.H.; Booij, N. A third-generation wave model for coastal regions: 2. Verification. *J. Geophys. Res.* **1999**, *104*, 7667–7681. [CrossRef]

42. Amarouche, K.; Akpınar, A.; Bachari, N.E.I.; Çakmak, R.E.; Houma, F. Evaluation of a high-resolution wave hindcast model SWAN for the West Mediterranean basin. *Appl. Ocean Res.* **2019**, *84*, 225–241. [CrossRef]

43. Amarouche, K.; Akpınar, A.; El Islam Bachari, N.; Houma, F. Wave energy resource assessment along the Algerian coast based on 39-year wave hindcast. *Renew. Energy* **2020**. [CrossRef]

44. Saha, S.; Moorthi, S.; Pan, H.-L.; Wu, X.; Wang, J.; Nadiga, S.; Tripp, P.; Kistler, R.; Woollen, J.; Behringer, D.; et al. The {NCEP} Climate Forecast System Reanalysis. *Bull. Am. Meteorol. Soc.* **2010**, *91*, 1015–1058. [CrossRef]

45. Saha, S.; Moorthi, S.; Wu, X.; Wang, J.; Nadiga, S.; Tripp, P.; Behringer, D.; Hou, Y.-T.; Chuang, H.; Iredell, M.; et al. The {NCEP} Climate Forecast System Version 2. *J. Clim.* **2014**, *27*, 2185–2208. [CrossRef]

46. Tiberi-Wadier, A.-L.; Laugel, A.; Benoit, M. Construction of the Numerical Wave Databases Anemoc-2 on the Mediterranean Sea and the Atlantic Ocean Through Hindcast Simulations Over the Period 1979–2010. In *Advances in Hydroinformatics*; Springer Water; Springer: Singapore, 2016; pp. 127–143.

47. Campos, R.M.; Guedes Soares, C. Assessment of three wind reanalyses in the North Atlantic Ocean. *J. Oper. Oceanogr.* **2017**, *10*, 30–44. [CrossRef]

48. Campos, R.M.; Guedes Soares, C. Comparison and assessment of three wave hindcasts in the North Atlantic Ocean. *J. Oper. Oceanogr.* **2016**, *9*, 26–44. [CrossRef]

49. Stopa, J.E.; Cheung, K.F. Intercomparison of wind and wave data from the ECMWF Reanalysis Interim and the NCEP Climate Forecast System Reanalysis. *Ocean Model.* **2014**, *75*, 65–83. [CrossRef]

50. Carvalho, D. An assessment of NASA's GMAO MERRA-2 reanalysis surface winds. *J. Clim.* **2019**, *32*, 8261–8281. [CrossRef]

51. Akpinar, A.; Ponce de León, S. An assessment of the wind re-analyses in the modelling of an extreme sea state in the Black Sea. *Dyn. Atmos. Ocean.* **2016**, *73*, 61–75. [CrossRef]

52. Çakmak, R.E.; Akpinar, A.; Van Vledder, G.P. Comparative Performance Analysis of Different Wind Fields in Southern and North-Western Coastal Areas of the Black Sea. *Mediterr. Mar. Sci.* **2019**, *20*, 427–452. [CrossRef]

53. Van Vledder, G.P.; Akpınar, A. Wave model predictions in the Black Sea: Sensitivity to wind fields. *Appl. Ocean Res.* **2015**, *53*, 161–178. [CrossRef]

54. Cavaleri, L.; Rizzoli, P.M. Wind wave prediction in shallow water: Theory and applications. *J. Geophys. Res* **1981**, *86*, 10961–10973. [CrossRef]

55. Komen, G.J.; Hasselmann, K.; Hasselmann, K. On the Existence of a Fully Developed Wind-Sea Spectrum. *J. Phys. Oceanogr.* **1984**, *14*, 1271–1285. [CrossRef]

56. Janssen, P.A.E.M. Quasi-linear Theory of Wind-Wave Generation Applied to Wave Forecasting. *J. Phys. Oceanogr.* **1991**, *21*, 1631–1642. [CrossRef]

57. Janssen, P.A.E.M. Wave-Induced Stress and the Drag of Air Flow over Sea Waves. *J. Phys. Oceanogr.* **1989**, *19*, 745–754. [CrossRef]

58. Hasselmann, S.; Hasselmann, K. Computations and Parameterizations of the Nonlinear Energy Transfer in a Gravity-Wave Spectrum. Part I: A New Method for Efficient Computations of the Exact Nonlinear Transfer Integral. *J. Phys. Oceanogr.* **1985**, *15*, 1369–1377. [CrossRef]

59. Eldeberky, Y. *Nonlinear Transformations of Wave Spectra in the Nearshore Zone*; Delft University of Technology: Delft, The Netherlands, 1996.

60. Battjes, J.A.; Janssen, J.P.F.M. Energy Loss and Set-Up Due to Breaking of Random Waves. In Proceedings of the 16th International Conference on Coastal Engineering, Hamburg, Germany, 27 August–3 September 1978; American Society of Civil Engineers: New York, NY, USA, 1978; pp. 569–587. [CrossRef]

61. Hasselmann, K.; Barnett, T.P.; Bouws, E.; Carlson, H.; Cartwright, D.E.; Enke, K.; Ewing, J.A.; Gienapp, H.; Hasselmann, D.E.; Kruseman, P.; et al. Measurements of wind-wave growth and swell decay during the Joint North Sea Wave Project ({JONSWAP}). *Dtsch. Hydrogr. Z* **1973**, *A8*, 1–95.

62. Gusella, V. Estimation of extreme winds from short-term records. *J. Struct. Eng.* **1991**, *117*, 375–390. [CrossRef]

63. Nicholls, R.J.; Hoozemans, F.M.J. The Mediterranean: Vulnerability to coastal implications of climate change. *Ocean Coast. Manag.* **1996**, *31*, 105–132. [CrossRef]

64. Quevauviller, P. (Ed.) *Hydrometeorological Hazards*; John Wiley & Sons, Ltd.: Chichester, UK, 2014; Volume 1, ISBN 9781118629567. [CrossRef]

65. Guisado-Pintado, E.; Malvárez, G.; Navas, F.; Carrero, R. Spatial distribution of storm wave energy dissipation for the assessment of beach morphodynamics. *J. Coast. Res.* **2014**, *70*, 259–265. [CrossRef]

66. Karunarathna, H.; Pender, D.; Ranasinghe, R.; Short, A.D.; Reeve, D.E. The effects of storm clustering on beach profile variability. *Mar. Geol.* **2014**, *348*, 103–112. [CrossRef]

67. Sen, P.K. Estimates of the Regression Coefficient Based on Kendall's Tau. *J. Am. Stat. Assoc.* **1968**, *63*, 1379. [CrossRef]

68. Theil, H. A rank-invariant method of linear and polynomial regression analysis, Part I. *Proc. R. Neth. Acad. Sci.* **1950**, *53*, 387–392.

69. Kendall, M. *Rank Correlation Methods*, 4th ed.; Griffin: London, UK, 1975; ISBN 9780852641996.

70. Mann, H.B. Nonparametric Tests against Trend. *Econometrica* **1945**, *13*, 245. [CrossRef]

71. Cattrell, A.D.; Srokosz, M.; Moat, B.I.; Marsh, R. Seasonal intensification and trends of rogue wave events on the US western seaboard. *Sci. Rep.* **2019**, *9*. [CrossRef]

72. Yang, S.; Oh, J. Long-Term Changes in the Extreme Significant Wave Heights on the Western North Pacific: Impacts of Tropical Cyclone Activity and ENSO. *Asia-Pac. J. Atmos. Sci.* **2018**, *54*, 103–109. [CrossRef]

73. Nchaba, T.; Mpholo, M.; Lennard, C. Long-term austral summer wind speed trends over southern Africa. *Int. J. Climatol.* **2017**, *37*, 2850–2862. [CrossRef]

74. De Leo, F.; De Leo, A.; Besio, G.; Briganti, R. Detection and quantification of trends in time series of significant wave heights: An application in the Mediterranean Sea. *Ocean Eng.* **2020**, *202*, 107155. [CrossRef]

75. De Leo, F.; Besio, G.; Mentaschi, L. Trends and variability of ocean waves under RCP8.5 emission scenario in the Mediterranean Sea. *Ocean Dyn.* **2020**, 1–21. [CrossRef]

76. Aydoğan, B.; Ayat, B. Spatial variability of long-term trends of significant wave heights in the Black Sea. *Appl. Ocean Res.* **2018**, *79*, 20–35. [CrossRef]

77. Akpınar, A.; Bingölbali, B. Long-term variations of wind and wave conditions in the coastal regions of the Black Sea. *Nat. Hazards* **2016**, *84*, 69–92. [CrossRef]

78. Martzikos, N.T.; Prinos, P.E.; Memos, C.D.; Tsoukala, V.K. Statistical analysis of Mediterranean coastal storms. *Oceanologia* **2020**. [CrossRef]

79. Cavicchia, L.; von Storch, H.; Gualdi, S. A long-term climatology of medicanes. *Clim. Dyn.* **2014**, *43*, 1183–1195. [CrossRef]

80. Young, I.R.; Zieger, S.; Babanin, A.V. Global trends in wind speed and wave height. *Science* **2011**, *332*, 451–455. [CrossRef] [PubMed]

81. Timmermans, B.W.; Gommenginger, C.P.; Dodet, G.; Bidlot, J.-R. Global Wave Height Trends and Variability from New Multimission Satellite Altimeter Products, Reanalyses, and Wave Buoys. *Geophys. Res. Lett.* **2020**, *47*. [CrossRef]

82. Shanas, P.R.; Kumar, V.S. Trends in surface wind speed and significant wave height as revealed by ERA-Interim wind wave hindcast in the Central Bay of Bengal. *Int. J. Climatol.* **2015**, *35*, 2654–2663. [CrossRef]

83. Wang, X.L.; Swail, V.R. Trends of Atlantic Wave Extremes as Simulated in a 40-Yr Wave Hindcast Using Kinematically Reanalyzed Wind Fields. *J. Clim.* **2002**, *15*, 1020–1035. [CrossRef]

84. Aarnes, O.J.; Abdalla, S.; Bidlot, J.-R.; Breivik, Ø. American Meteorological Society Marine Wind and Wave Height Trends at Different ERA-Interim Forecast Ranges. *Source J. Clim.* **2015**, *28*, 819–837. [CrossRef]

85. Divinsky, B.V.; Kosyan, R.D. Climatic trends in the fluctuations of wind waves power in the Black Sea. *Estuar. Coast. Shelf Sci.* **2020**, *235*, 106577. [CrossRef]